Archives of Civil and Mechanical Engineering (2023) 23:102
https://doi.org/10.1007/s43452-023-00636-4

ORIGINAL ARTICLE

Forging of PM Ti–6Al–4V alloy at the temperature above β-transus and high strain rate: modeling and trials in industrial conditions

Marek Wojtaszek[1] · Krystian Zyguła[1] · Aneta Łukaszek-Sołek[1] · Magdalena Jabłońska[2] · Rafał Stanik[3] · Maik Gude[3]

Received: 5 January 2023 / Revised: 27 February 2023 / Accepted: 12 March 2023 / Published online: 25 March 2023

Abstract

The results of the forging process in open dies of the powder metallurgy (PM) Ti–6Al–4V alloy, carried out at the temperature above β-transus and at a high strain rate were presented. As an initial material for the research relatively cheap elemental powders were used. This approach gives a real chance for the implementation of the developed technologies. As the range of phase transition temperature in titanium alloys is influenced also by the technology of their production, the β-transus temperature was estimated for the PM Ti–6Al–4V alloy. Finite element method (FEM) numerical analysis of the forging process at the temperature of 1000 °C and high strain rate was performed. The results obtained by the FEM modeling were verified under industrial conditions. The forging trials were made at the temperature of 1000 °C on a screw press operating at a speed of 250 mm s^{-1}. For comparison, the alloy was also studied in as-cast and hot-rolled conditions, which is widely used as a feedstock. The influence of the method of manufacturing feedstock on the microstructure and selected properties of the forgings was determined. This approach allowed for a qualitative assessment of the PM material. The forging process in open dies of two different feedstocks led to the production of forgings with a uniform and similar lamellar microstructure. Thus, it was shown that the heating conditions, the parameters of the forging process, and the method of cooling the product after forging have a decisive influence on the microstructure condition of the forgings shaped in the temperature range of the β phase.

Keywords Ti–6Al–4V alloy · Powder metallurgy · Open-die forging · Microstructure · β-Transus temperature

1 Introduction

Titanium alloys have been considered unique materials for many years [1]. They are mainly used in transportation, machine building, shipbuilding [2], the fuel–energy industry, and medicine [3]. The main reason for that is favorable combination of properties, such as good creep resistance [4], excellent strength [5] and high fatigue performance [6]. These materials are also resistant to high-temperature failure [7]. Some titanium alloys are biocompatible and resistant to corrosion in a biological environment [8], which enables their use for dental applications [9] and in the manufacture of implants, including fracture fixation, hip joint replacement [10]. The advantage of titanium alloys is also the ability to extensive control of their microstructure, which can be achieved in the processes of melting and crystallization, plastic processing, and heat treatment [11]. The disadvantages of titanium alloys include mainly difficulties in machining [12], low thermal conductivity [13], and high material and fabrication costs [14]. Therefore, titanium applications are limited to products where high properties are critical, and cost is of a less important [15]. Currently, a semi-finished product in the form of a hot deformed casting is commonly used to produce structural components from titanium alloys [16]. However, it is believed that the implementation of a new, less expensive and more efficient production process of titanium sponge and technologies to minimize the extremely costly mechanical working, like powder technologies or near-net-shape technologies, is the key to

✉ Marek Wojtaszek
wojtaszek@agh.edu.pl

[1] Faculty of Metals Engineering and Industrial Computer Science, AGH University of Science and Technology, Al. A. Mickiewicza 30, 30-059 Kraków, Poland

[2] Faculty of Materials Engineering, Silesian University of Technology, Krasińskiego 8, 40-019 Katowice, Poland

[3] Institute of Lightweight Engineering and Polymer Technology (ILK), Technische Universität Dresden, Holbeinstraße 3, 01307 Dresden, Germany

unlock the huge application potential of titanium or titanium alloys [17]. Another way to decrease cost is to reduce the number of processing steps from ore to component [18]. Recently, for this purpose, new technologies of manufacturing products from aluminum alloy powders, such as additive manufacturing (AM), have also been introduced [19].

The most widely used titanium alloy is the two-phase Ti–6Al–4V alloy. In addition to the advantages specific to titanium, it exhibits heat resistance and weldability [16], high strength under dynamic loading conditions [20], impact toughness [21], as well as good mechanical behavior under quasi-static and dynamic loads [22]. Another very important advantage of this alloy is its potential for hot plastic deformation. It allows manufacturers to manufacture products from this alloy using commercial hot-forming processes, mainly forging [23], rolling [24], or extrusion [25]. This usually applies to the typical feedstock in the form of a hot processed casting, and semi-finished products obtained by alternative methods, including powder metallurgy [26]. To determine the advantages and disadvantages of this approach, the microstructure and properties of products obtained using typical feedstock and semi-finished products manufactured by alternative ways are compared [27]. In the case of using a feedstock made with an alternative technology, it is necessary to determine the favorable parameters of its hot plastic processing [28]. In recent years, advanced research has been carried out on the possibility of using titanium alloys made from powders as semi-finished products for hot forming. They are carried out by scientific centers and by the research and development departments cooperating with commercial companies. For example, Qiu et al. [29] presented the results of research that aimed to select the most favorable parameters for the hot forging process of connecting rods made of powders. Kanou et al. [30] addressed the problem of modifying the mechanical properties of the Ti–6Al–4V alloy by Fe addition. They showed that the Ti alloys obtained in this study have a strong potential for application in automobiles and aircraft. Liang et al. [31] focused on the study of the microstructure and tensile properties of a rod and disc made of the Ti–6Al–4V alloy fabricated by the methods of extrusion and forging of the feedstock obtained from the powder. Jia et al. [32] manufactured the rocker arms for internal combustion engines using the method of fast forging of Ti–6Al–4V powder into near-net-shaped parts. The ADMA Products, Inc. developed a technology based on the processing of the Ti–6Al–4V alloy obtained by powder metallurgy, the purpose of which was to produce profiles that meet the requirements for responsible structures in aviation [33]. In the work [34] Froes characterized various technological paths based on hot metal forming which led to full densification of Ti–6Al–4V sinters. The obtained products were used commercially, among others in medicine and in the defense industry. Some of the above-mentioned works consider the fact that during hot deformation the changes in the proportions of the various phases depend both on temperature and on the time of exposure to temperature, which is mainly due to the strain rate. As a result, by properly selecting the temperature and strain rate, it is possible to control the microstructure and modify the properties [35]. However, even at high temperatures, the range of parameters in which the alloy exhibits sufficient formability for being deform without risk of failure is limited [36]. This is particularly applicable to hot forming using high strain rates [37]. For this reason, a requirement for the correct design of a specific hot-forming process for Ti–6Al–4V alloy is the proper selection of the right combination of temperature, strain rate and strain value. It should be taken into account that titanium has two allotropic forms: at low temperature there is a Ti_{α} crystalline phase, having a hexagonal closed packed (HCP) structure. At high temperatures, there is a Ti_{β} crystalline phase that has a body-centered cubic structure (BCC). In the case of titanium alloys, the relative volume of the α and β phases is influenced by the temperature and the content of the alloying elements. Therefore, two different approaches are used in industrial practice to define the temperature ranges of the forging process of the Ti–6Al–4V alloy [38]. The choice of one of them leads to obtaining a microstructure with the desired morphology; equiaxed, bimodal, or lamellar [37]. The first approach involves forging in a range below the β-transus temperature, which for the Ti–6Al–4V alloy obtained by casting processes is about 995 °C. This leads to an equiaxed microstructure, consisting of equiaxed grains of both phases, or a bimodal microstructure, consisting of equiaxed grains of the α phase in a matrix composed of α and β phase plates. This microstructure results in forged products with a very good combination of strength and fatigue properties. That is why forming below the β-transus temperature is used much more often. The second approach involves forging in the temperature range above the phase transformation temperature. As a result, the microstructure is transformed to the β phase. After forging under such conditions and subsequent cooling of the forging at natural speed, a lamellar microstructure is formed in the transformed matrix, called a Widmanstätten microstructure [39]. The benefits of obtaining such a microstructure are mainly excellent specific strength, fracture toughness, and resistance to crack propagation [40]. The disadvantage of the products obtained in this way is poor toughness [41].

Depending on the purpose of the component being produced and the required properties, either the first or second approach is used in industry. Over the past few years, several studies have been conducted to understand the mechanisms occurring during the hot deformation of titanium alloys and the evolution of their microstructure. The subject of much of the work carried out in this area has been the alloy Ti–6Al–4V [42, 43]. The influence of strain temperature was evaluated in

terms of selecting the most favorable parameters for the forming processes of this alloy, such as forging or extrusion [24]. The study also included processes conducted at high strain rates [44]. However, these works have mainly focused on the Ti–6Al–4V alloy in the form of a deformed casting, which is now widely used as a feedstock for plastic processing.

The results of studies on the effect of hot-forming parameters on the microstructural state of Ti–6Al–4V alloy products made by powder metallurgy methods are published much less frequently. Furthermore, most of the information described in the literature relates to the forming of this type of material in terms of the coexistence of α and β phases. These data can be found in the work on issues such as the hot forging process parameters by Qiu et al. [29] and the ring rolling of powder compacts conducted by Guo et al. [45]. However, there are no comprehensive data on the forming processes of these materials carried out in the temperature range higher than the β-transus temperature. It should also be taken into account that the kinetics of phase transformations of titanium alloys is affected not only by their chemical composition but also by the technology of their manufacture. Taking as their motivation the need to supplement the mentioned information, in this paper, the authors present the results of the thermal analysis leading to the estimation of $\alpha+\beta\leftrightarrow\beta$ transus temperature of the Ti–6Al–4V alloy produced by the original method from elementary powders, as well as the flow curves developed based on compression tests under controlled conditions. These data provided the basis for describing the material, which was necessary to carry out numerical modeling by the finite element method (FEM) of the forging process of an example forging from this material. The forging process was analyzed at high speed and the temperature of β-phase occurrence. In the next stage, the correctness of the obtained results was verified based on technological tests on the industrial line and by performing tests on the properties of the forgings. In addition, under the same conditions, a commercial, hot deformed casting was forged and regarded as a reference material for evaluating the quality of forgings produced by powder metallurgy. It was assumed that the result of the planned research would be the development of guidelines for the implementation of the forging process in the β-phase range and at a high strain rate of the Ti–6Al–4V alloy charge obtained from elementary powders. Application of these guidelines to a commercial hot forging line will allow for the production of defect-free forgings with a controlled and favorable microstructure.

2 Experimental procedure

2.1 Examined materials

The Ti–6Al–4V alloy used for this study was manufactured by hot pressing a mixture of elemental powders. As the reference material, the standard Ti–6Al–4V feedstock produced in the processes of casting and hot rolling was used. This material is currently widely used both to produce structural parts by machining and as the stock for hot processing.

Manufacturing of Ti–6Al–4V alloy by powder metallurgy The starting materials for the study were titanium, aluminum, and vanadium powders, in amounts suitable to produce Ti–6Al–4V alloy. It was taken into account that the minimum and maximum contents of basic alloying elements required for the Ti–6Al–4V alloy are, respectively: aluminum: 5.50–6.75, vanadium: 3.5–4.5 and titanium: balance. Titanium and vanadium powders with irregular particle shapes and sizes below 150 µm (mesh class 100) were used. In the case of aluminum powder with a particle size below 45 µm (mesh class 325) was used.

The powders were mixed in a ceramic chamber in the presence of tungsten carbide balls. The mixing process was carried out for 120 min at a speed of 55 rpm. The quality of the mixture was checked by Energy-Dispersive X-ray Spectroscopy (EDS) using a Hitachi TM-3000 (Hitachi, Ltd., Tokyo, Japan) scanning microscope. Particles of individual powders were identified, which allowed qualitative evaluation of the uniformity of their distribution and recognition of the effects occurring during mixing. Semi-finished products from the powder mixture intended for plastic processing were made by hot pressing (Thermal Technology Press Inc.). The process was carried out at a temperature of 1200 °C, for 2 h, under a pressure of 25 MPa and in a protective atmosphere of argon. Cylindrical semi-finished products with a diameter of 78 mm and a weight of about 1 kg were obtained.

2.2 Methods of investigation

Metallographic examination of sintered alloy and forgings by light microscopy was carried out on a Leica DM4000M (Leica Microsystems GmbH, Wetzlar, Germany) light microscope. Samples for observation were prepared with a standard grinding and polishing procedure and etched in two stages: first stage: 6% HF + 96% H_2O, second stage: 2% HF + 2% HNO_3 + 96% H_2O.

The chemical composition of the alloy was analyzed by melting in an inert gas atmosphere, using the following instruments: LECO R016—for the determination of total oxygen and N-Leco TN14—for the determination of total nitrogen, and by the XRF method, using a Niton XL3t analyzer—for the determination of the amount of other elements.

The study of the mechanical properties included tensile tests (Zwick-Roell GmbH & Co. KG, Ulm, Germany) and Vickers hardness tests (Zwick tester-Zwick GmbH, Ulm, Germany), conducted under a load of 19.6 N.

Dilatometric tests of Ti–6Al–4V alloy were conducted to evaluate the behavior of the sintered alloy during heating and cooling using Linseis L78 RITA (Rapid Induction Thermal Analysis). Particular attention was paid to the analysis of the $\alpha+\beta \leftrightarrow \beta$ phase transformation. During testing ϕ 3 mm × 10 mm cylindrical samples were used. The samples were heated at a rate of 2.5 °C s^{-1} to 1100 °C, held for 5 s, and then cooled at a rate of 2.5 °C s^{-1} to room temperature. Dilatograms were analyzed using the differential curve method.

Quantitative analysis of the proportion of alpha and beta phases as a function of temperature was performed at temperatures of 950, 975, 1000, 1010, 1020, and 1030 °C, respectively. Samples of ϕ 10 mm × 6 mm were placed in an oven heated to the assigned temperature and held there for 10 min, then cooled at a high rate to maintain the microstructure in the state immediately after heat treatment. Microstructure images were taken in cross-sections at randomly selected locations in the center zone of the sample. The quantitative microstructure analysis software Leica Application Suite v. 4.8, was used to estimate the shares of α and β phases in the volume of the sintered alloy.

The hot compression tests were carried out on the Thermal–Mechanical Physical Simulation System Gleeble 3800 (Dynamic Systems Inc, Poestenkill, NY, USA). Cylindrical samples with dimensions ϕ 10 mm × 12 mm were resistively heated at 2.5 °C s^{-1} to the assigned temperature, held at this temperature for 10 s, and then compressed at a constant strain rate. The compression tests were conducted at 1000 °C, using strain rates in the range of 0.01–100 s^{-1} and a constant strain value of $\varepsilon = 1$. After deformation, the samples were cooled at a high rate using compressed air.

Numerical FEM simulations of the forging process in open dies were carried out using the QForm 3D software. During modeling, the material was considered an incompressible isotropic continuum. The elastic deformation range was not considered. The software performed calculations based on a rigid-viscous model with reinforcement, according to which the flow stress is dependent on the amount of deformation, the strain rate, and the temperature. The heat generated during plastic deformation was also included in the calculations, which is important when modeling processes carried out at high strain rates. Levanov's first law was used to describe friction. To describe the rheology of the material, flow curves developed based on plastometric tests, and thermal characteristics of materials determined based on the results of the publication co-author's original research, were implemented into the QForm program.

Forging tests were performed at Belos Preformed Line Products S.A Bielsko Biala, Poland. The forging feedstock was a Ti–6Al–4V alloy obtained by the powder metallurgy-based method proposed in the paper, and a hot deformed casting, which was the reference material. The same feedstock dimensions and process conditions were used for both compared materials. Forging was carried out on a screw press with a maximum upper tool speed of 250 mm s^{-1}. The shape and dimensions of the forging were determined by FEM modeling. A cylindrical feedstock with a diameter of 40 mm and a height of 37 mm was used for testing. The samples were coated with GL7120 grease and deltaforge F-31 grease was used to lubricate the dies. The dies were heated to 250 °C. The temperature of the dies and the feedstock were controlled continuously using pyrometers. The feedstock was heated in a GRC50 induction heater to 1000 °C, then transported to the die. The forging process was carried out in one operation. The forgings were cooled in the air.

Non-destructive testing was performed by Computed Tomography (CT). A v|tome|x L-450 CT scanner was used, which allows scanning objects with a maximum diameter of 1000 mm, a height of 2500 mm, and a mass of up to 200 kg. To view the images and analyze them, VGL 2.1 software was used, which allows observing the images in any area of the forging, making 3-dimensional assemblies of them, and zooming the indicated areas. Images were archived at a resolution of 2014 × 2024 ppi. The symmetry of the forging's shape was used to increase the precision of the study. Only the part lying between two mutually perpendicular planes was scanned. The cutting of the forgings was carried out leaving an excess of 2 mm extending beyond the accepted symmetry limits, which made it possible to observe the internal structure of the forgings in the dividing planes. A significant part of the flash was removed from the specimens, leaving a trace of it to facilitate localization of the zone of transition of the forging into the flash. Minimizing the size of the object made it possible to perform CT examinations in two mutually perpendicular directions with a resolution of 15 µm. In addition, rotational scanning of the forgings was performed, taking as the axis of rotation the axis coinciding with the line of intersection of the dividing planes. The angle between consecutive scanned surfaces was 0.25°.

3 Results

3.1 EDS analysis of powder mixture

The morphology of the powder mixture and example results of EDS analysis are summarized in Fig. 1. Soft aluminum powder particles were observed on the surfaces of larger and harder titanium and vanadium powder particles (Fig. 1b–e). Vanadium was present in the form of powder particles and fragments of these particles, were crushed and inserted to the surface of titanium particles (Fig. 1e).

3.2 Characteristics of as-sintered Ti–6Al–4V alloy

In Table 1, the chemical composition of as-sintered Ti–6Al–4V alloy was presented. A fairly high oxygen content is a result of the technological path used to produce of the sintered alloy, primarily the conditions of the mixing process.

Figure 2a shows the microstructure of the sintered alloy. It has a lamellar structure, consisting of massive lamellae of α phase (light phase visible at low magnification) in a matrix of β phase (darker phase) and α phase precipitates located at the former grain boundaries of β phase. Observations revealed the presence of a few pores of small size and spherical shape. The slight relative porosity found (about 0.6%) was confirmed by the results of the observations of the microstructure of the sintered alloy. The yield strength of the sintered alloy determined by the tensile test was 950 ± 26 MPa and the

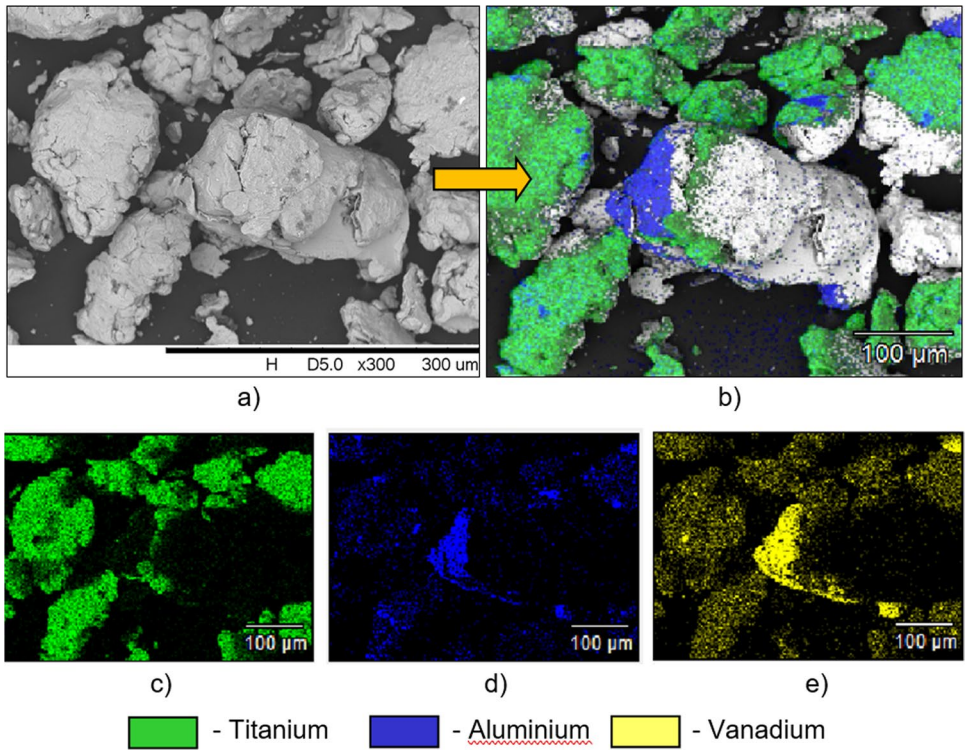

Fig. 1 Results of the study of the mixture of elemental powders: **a** morphology of the mixture, **b–e** identification by EDS of the chemical composition of the particles and their distribution in the mixture

Table 1 Chemical composition of PM Ti–6Al–4V alloy

Chemical element	Al	V	Fe	Cu	Mn	Cr	O	N	Ti
Content, wt.%	5.50	4.15	0.33	0.01	0.09	0.01	0.025	0.002	Balance

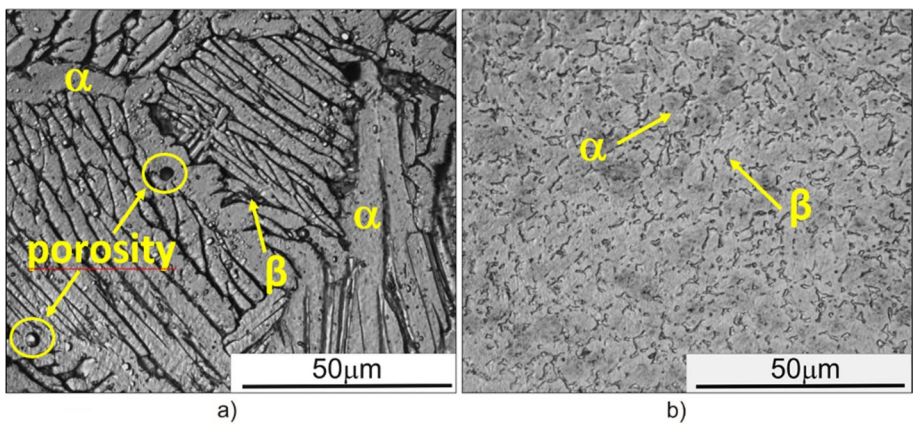

Fig. 2 Microstructure of Ti–6Al–4V alloy—the cross-sections of sintered (**a**) and hot-rolled (**b**) feedstocks

Young's modulus of this material was 121 ± 16 GPa. The average tensile strength obtained for the sintered alloy was 1022 ± 24 MPa and the relative elongation was 5.9 ± 0.9%. The hardness of the sintered alloy was 338 ± 3 HV_2.

3.3 Characteristics of the hot-rolled casting of Ti–6Al–4V alloy

Following the objectives of this work, the results of the hot forging of moldings in open dies were compared with the results of tests conducted on a reference material, which was a hot-rolled casting of Ti–6Al–4V alloy. In the as-delivered condition, it had a rod shape with a diameter of 50.8 mm. Figure 2b shows a microstructure of the hot-rolled casting in the delivery state. It consists of equiaxial α phase grains and β phase grains lying on the boundaries of the α grains. The yield strength determined in the tensile test was 978 ± 18 MPa, Young's modulus was 108 ± 19 GPa and UTS was 1017 ± 22 MPa. The elongation value of the tested material was 13.5 ± 3.1%. The hardness of the reference material was 317 ± 3 HV_2.

3.4 Determination of the phase transformation temperature of Ti–6Al–4V alloy

The temperature of the phase transformation α + β ↔ β in titanium alloys is influenced not only by their chemical composition but also by the technology of their manufacture. Therefore, a study was undertaken to estimate the end temperature of the phase transformation of sintered alloy made of the Ti–6Al–4V alloy.

3.4.1 Dilatometric studies of as-sintered Ti–6Al–4V alloy

Figure 3 summarizes the dilatometric curves obtained from the heating and cooling of the sintered alloy and a photograph of the microstructure of the samples after the dilatometric tests.

The differential curve developed for heating (Fig. 3a) shows a slight increase in the temperature range from 300 to 400 °C. Beyond 700 °C, inhibition of the growth rate of the sample length is observed, indicating a wide range of α + β ↔ β phase transformation. Therefore, the temperature of the end of the α + β ↔ β phase transformation was not precisely determined based on dilatometric studies. Nevertheless, microstructural tests carried out on the sample after cooling the sample in the dilatometric test indicate the occurrence of the α + β → β transformation in the entire volume of the material (Fig. 3c). Estimated from the dilatometric curve (Fig. 3b), the approximate temperatures of the beginning and end of the transformation under the adopted cooling conditions are about 965 °C and 780 °C, respectively. Observations of the microstructure of the samples subjected to dilatometric tests were carried out on their cross-sections. The microstructure obtained as a result of tests conducted up to 1100 °C (Fig. 3c) has a lamellar structure. It consists of fine lamellae of the α phase (light phase) inside the β phase (dark phase) located inside the primary grains of the β phase, occurring when the sample is exposed at temperatures above the α + β ↔ β phase transformation temperature, and continuous α phase precipitates are located at the former β/β grain boundaries. The α-phase lamellae visible in the image, as well as the separations of this phase at the grain boundaries, are thin, especially when compared with the material in the hot-pressed state (Fig. 1a), where the microstructure components are massive.

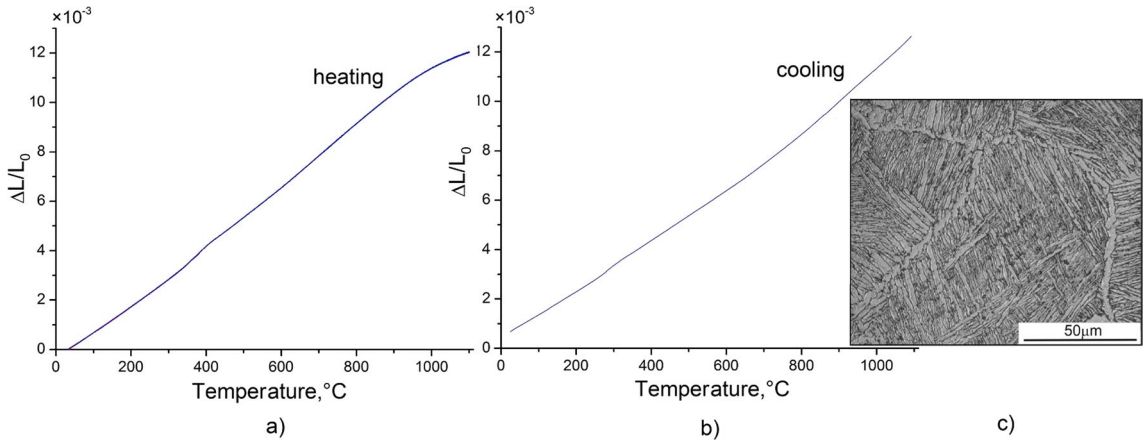

Fig. 3 Dilatometric curves obtained for sintered Ti–6Al–4V alloy during: **a** heating at a rate of 2.5 °C s^{-1}, **b** cooling at a rate of 2.5 °C s^{-1} and **c** microstructure after cooling

3.4.2 Effect of sintered alloy temperature on the contribution of α and β phases

Since the temperature of the end of the α + β ↔ β transformation could not be determined from the differential curve developed for the heating of sintered Ti–6Al–4V alloy, a quantitative analysis of the contributions of the α and β phases as a function of temperature was therefore carried out. Figure 4 shows the results of the quantitative analysis of the contributions of α and β phases to the volume of the sintered alloy, depending on the temperature. As a result of heating the sample to 975 °C, holding at this temperature, and rapid cooling, the α phase was found to be about 16.8%. Performing this procedure at temperatures of 1000 and 1010 °C resulted in the occurrence of the α phase in an amount of about 4%, quantitatively confirming the conclusions made based on the analysis of dilatometric curves. In the case of samples heated to temperatures in the range of 1020–1030 °C and cooled at a high rate, observations of their microstructure showed only insignificant amounts of α phase, for which reason their quantitative analysis was not carried out.

3.5 Physical modeling of hot forming of sintered Ti–6Al–4V alloy based on hot compression tests

The objective of hot compression tests on a Gleeble 3800 simulator was to determine and compare the behavior of the Ti–6Al–4V alloy in terms of the occurrence of the β-phase, depending on the strain rate. This considered the need to supplement information on the behavior of titanium alloys during their forming at high strain rates. Figure 5 shows the effect of the strain rate used during testing at 1000 °C on the true stress-true strain curves.

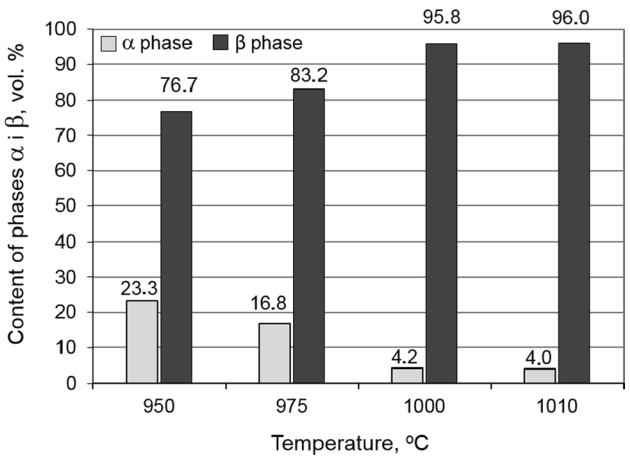

Fig. 4 Effect of temperature on volume contributions of α and β phases in the microstructure of a sintered alloy

The flow curve obtained from compression at a strain rate of 100 s^{-1} has an oscillatory pattern over the full strain range. The curves developed from compression tests at strain rates in the range of 1–100 s^{-1} show a decrease in true stress values with an increase in true strain over the full strain range. For low strain rates, the increase in true strain occurred with a slightly decreasing value of true strain. The obtained curves do not show a hardening effect and are essentially similar, both in shape and in the course as a function of strain, differing only in the values of the flow stress.

3.6 FEM simulation of die forging on a screw press

The finite element method (FEM) modeling of the hot die forging process of Ti–6Al–4V alloy semi-finished products obtained from elementary powders was carried out. A range of parameters and forging conditions was adopted that could be verified on an industrial line. For this reason, the modeling included conditions and limitations that occur during forging on industrially used stands. These included the transportation time of the feedstock from the furnace to the press, the heating and cooling conditions, and the tool temperatures that were achievable with the heating systems available at the forge plant. Numerical simulations were performed at a temperature suitable for the presence of a β-phase in the studied alloy and under conditions of relatively high strain rates. These conditions were obtained by running the process at 1000 °C and on a screw press operating at a maximum speed of 250 mm s^{-1}. The adopted temperature made it possible to realize forging in the upper range of the phase transformation and in a single technological procedure, which facilitated obtaining clear relationships between the deformation conditions and the microstructure and properties of the forgings.

A closed-form forging was selected for FEM analysis, the shape of which led to different flow conditions in different areas of the forging and provided the possibility of obtaining varying degrees of deformation in the volume of the

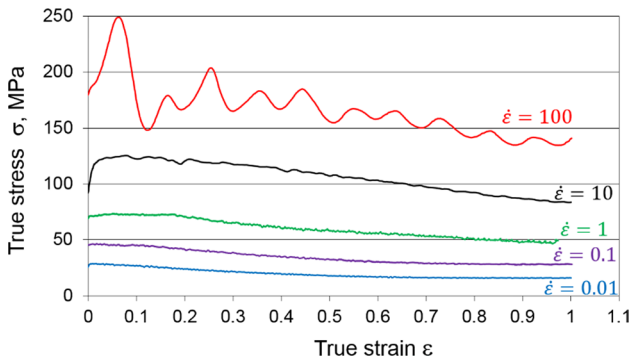

Fig. 5 Effect of strain rate of sintered Ti–6Al–4V alloy on true stress–strain curves developed from hot compression tests at 1000 °C

product. The shape and dimensions of the forging are shown in Fig. 6, and the shape of the lower and upper dies, in Fig. 7. A series of simulations were performed, assuming varying conditions that included the shape of the feedstock and the way it was positioned in the dies. Preliminary simulations showed that the geometry of the forging adopted allowed forging to be carried out in a single technological operation and at tool movement speeds in the range appropriate for screw presses. The selected shape was, during the realization of the research, serially produced in Poland (from a material other than titanium alloy), on an industrial production line, and, after machining, used in the power industry.

A feedstock in the shape of a cylinder with a diameter of 40 mm and a height of 37 mm was selected as the most favorable for the modeled alloy. Preliminary measurements were made in the forge plant to determine the possibilities and limitations when realizing the modeled tests under industrial conditions. The maximum possible temperatures of the lower and upper die were measured, which were 250 °C. These values were adopted during the simulations. The feedstock was modeled to be heated to 1000 °C, rapidly transported from the furnace to the bottom die, and the feedstock was forged in a single technological operation. The maximum speed of the upper die during forging was 250 mm s^{-1}. Based on the data on the lubricants used in the industry (feedstock—GL7120 grease, dies—deltaforge F-31 grease), the friction coefficient at the contact surface of the material and tools was estimated at 0.15. Example results of FEM calculations of the forging process in open dies of Ti–6Al–4V alloy obtained from powders are shown in Fig. 8.

The FEM analysis showed that during the hot forging process, forgings of the selected shape and under the modeled conditions lead to correct filling of the dies. No forging defects, such as laps, were found. The temperature distribution obtained from the FEM analysis at the final

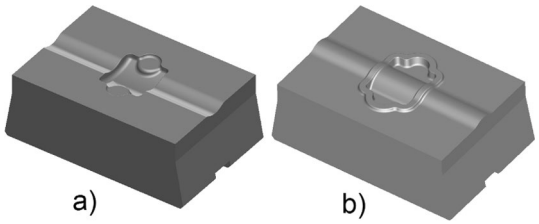

Fig. 7 Tool geometry: **a** lower die, **b** upper die

stage of the process (Fig. 8a, b) indicates that the temperature in almost the entire volume of the forging was fairly uniform as a result of the implementation of the assumed forging variant. Significant temperature increases are expected only in the area adjacent to the flash and in the flash zone (Fig. 8b). In the rest of the forging volume, the FEM analysis did not show temperature rises to values above 1080 °C. A slight temperature drop below 1000 °C in the final stage of the process occurred only in the zone near the feedstock's contact surface with the lower die (Fig. 8b). Slightly higher values of effective stress were found in this area (Fig. 8d). On the other hand, very high values of effective stress were observed in the zone adjacent to the flash and in part of the flash itself. Outside these areas in the volume of the forging, the value of effective stress was relatively low, in the range of 25–100 MPa (Fig. 8c, d). Positive mean stress values were found in the flash zone (Fig. 8f). Compressive stresses were observed in the rest of the forging (Fig. 8e, f). The largest negative values of these stresses were shown in the middle part of the forging, especially in the part shaped by the upper die and in the areas near the roundness of the die. In the transition zone between the forging and flash, the FEM analysis showed differences in mean stress values (Fig. 8e, f) and very large variations in plastic strain values (Fig. 8g, h). In the rest of the forging volume, the distribution of plastic strain values was fairly uniform.

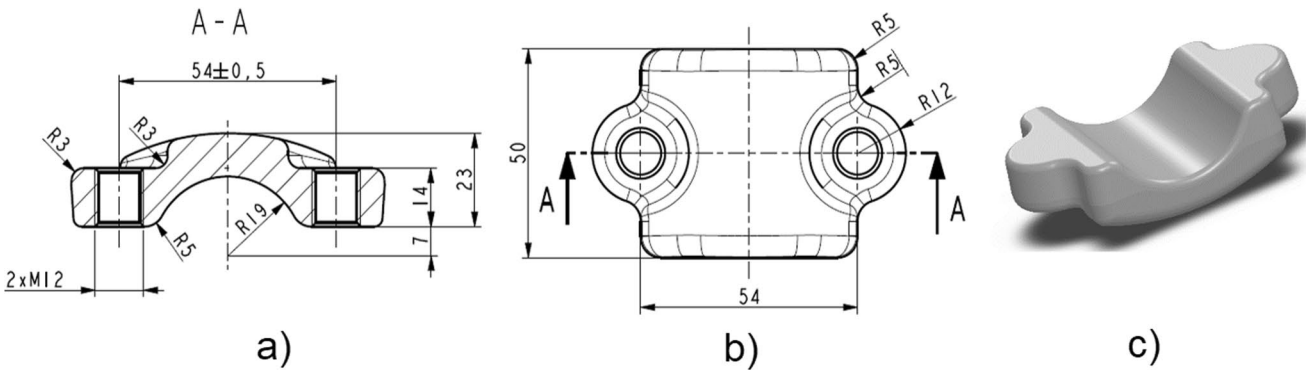

Fig. 6 Dimensions (**a**, **b**) and **c** model of the forging

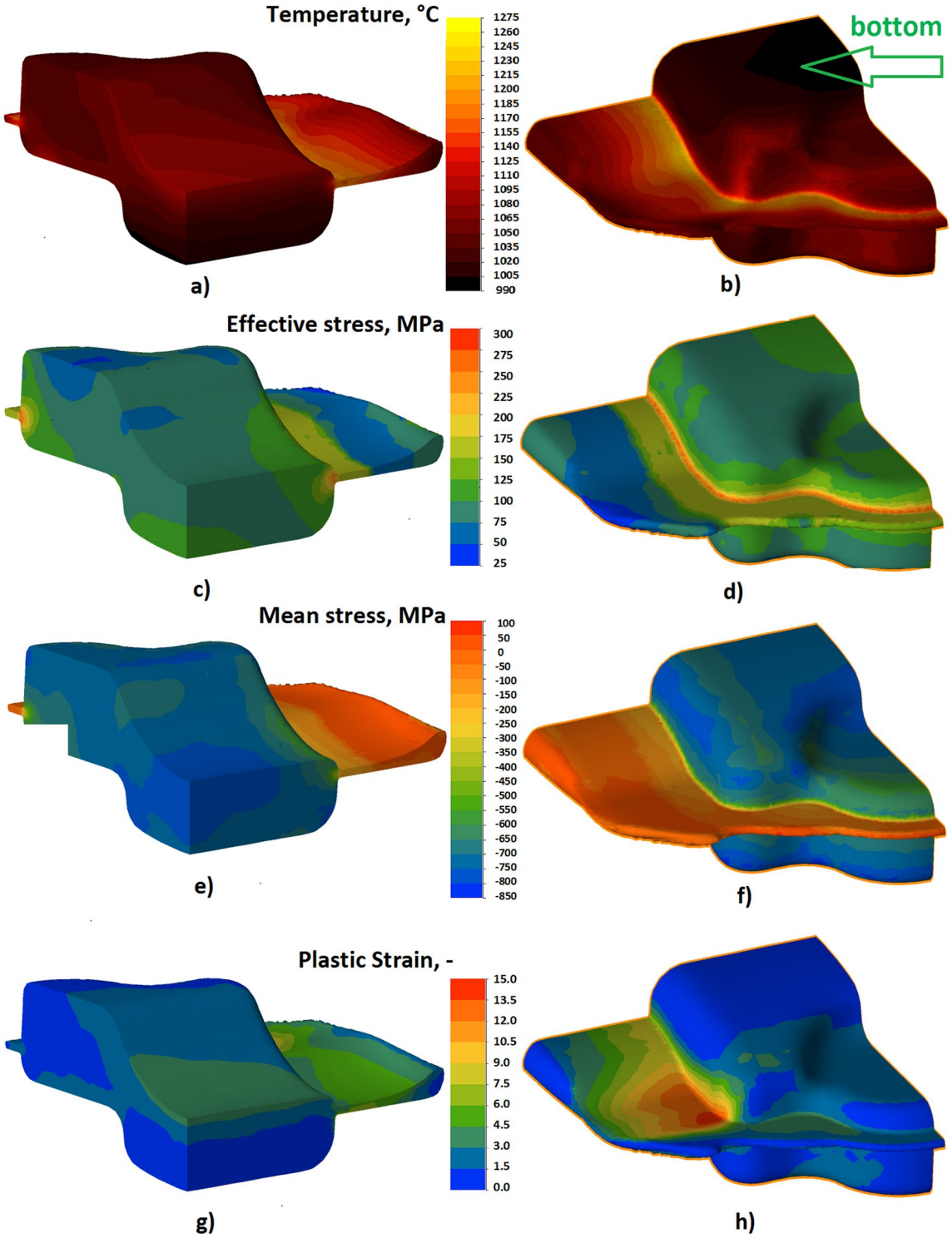

Fig. 8 FEM simulation results: **a**, **b** temperature, **c**, **d** effective stress, **e**, **f** mean stress, **g**, **h** plastic strain. The final stage of hot forging in open dies of sintered Ti–6Al–4V alloy: **a**, **c**, **e**, **g** part of the forging shaped by the upper die together with sections in the symmetry planes, **b**, **d**, **f**, **h** the underside of the forging with a visible zone of transition to the flash

3.7 Hot forging tests in open dies on a screw press

The correctness of the FEM analysis results was verified by performing forging tests under industrial conditions and then evaluating the microstructures and selected properties of the forgings. It was taken into account that in the case of materials used for the production of structural components, including the Ti–6Al–4V alloy, the condition for the implementation of alternative technology is not only the economic aspect but also the appropriate quality of the product, which must not differ from the quality of products obtained using commonly implemented processes. Therefore, in this part of the study, forging tests of Ti–6Al–4V alloy was conducted using not only a feedstock in the form of sintered alloy, but also a commercially used industrial semi-finished product in the form of a hot deformed casting, and its microstructure in the delivery state is shown in Fig. 2b. The microstructure of the two compared materials depended on their manufacturing method and differed significantly (Fig. 2a, b). However, due to the comparative purpose of the study, no preliminary heat treatment leading to its homogenization was performed.

The forging process was carried out on a screw press with a maximum upper tool speed of 250 mm s^{-1}. The die assembly is shown in Fig. 9a, and the lower die in Fig. 9b. Both of these figures show how the dies are heated with gas torches. The target shape and dimensions of the forging were developed during FEM modeling. The method of placing the feedstock on the lower die is shown in Fig. 9c. The process was carried out in a single operation. The shape of the forging immediately after deformation is shown in Fig. 9d.

3.8 Forging test results and their comparison

Immediately after forging and cooling, an initial visual evaluation was carried out. Observations showed no visible defects on their surfaces. It was found that forging in the β-phase range and with a high speed of tool movement resulted in the proper filling of both dies. Regardless of how the feedstock was made, products with the correct shape were obtained. Cracks were observed only in the flash zone of forgings made from both types of feedstock. However, this does not affect the quality of the products, since the flash is waste and is removed immediately after the forging process using a trimming press. The evaluation of the condition of the forgings at this stage indicated that the material obtained by powder metallurgy was suitable for further comparative studies. These studies included a preliminary visual assessment of the surface of the forgings, an evaluation of the internal structure of the forged sintered alloy, microstructure observations, and hardness measurements of forged products using both types of feedstock. In the case of products obtained by powder metallurgy, special attention was paid during the evaluation of the test results to those zones that were indicated as prone to the formation of defects during the analysis of the FEM modeling results. The results of microstructure and hardness tests of the two materials were compiled and compared, which enabled a qualitative evaluation of the product made from elemental powders.

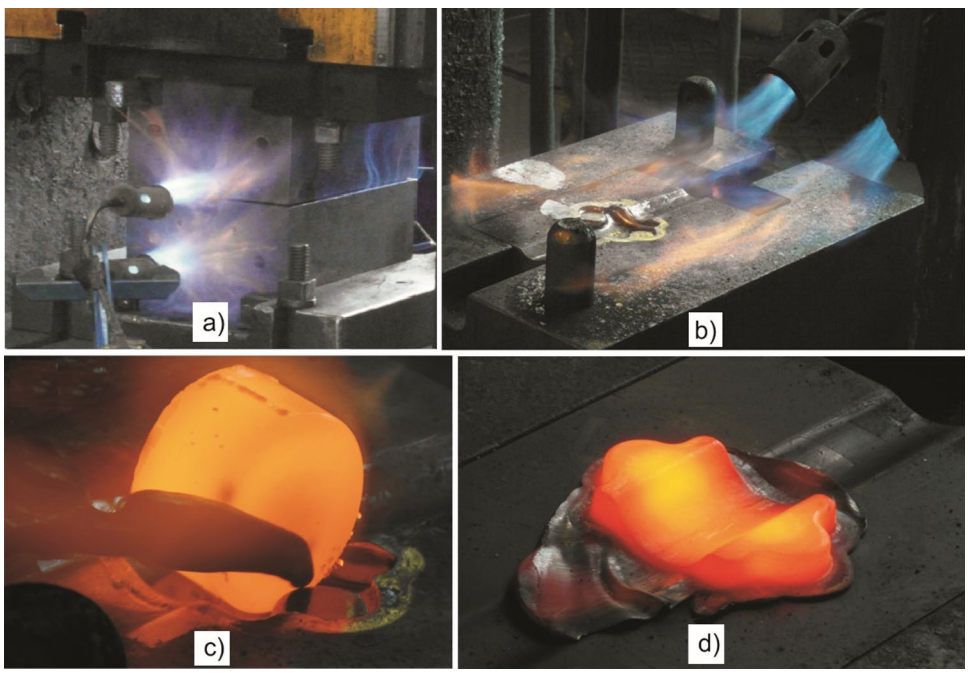

Fig. 9 Forging trials at BELOS PLP S.A.: **a** press nest with die heating, **b** bottom die, **c** way of placing feedstock heated to 1000 °C in the die, **d** forging (made from feedstock obtained by powder metallurgy)

3.8.1 CT nondestructive testing of sintered alloy after forging

Computed Tomography (CT) nondestructive testing was performed on a forging made by powder metallurgy technology. A resolution of 15 µm was used. Figures 10 and 11 summarize the selected CT results of the forging. The figures are accompanied by diagrams indicating the location of the section where the image was taken. The flash transition zones are marked with arrows in the figures. When analyzing the scans, special attention was paid to the continuity of those areas that were identified as critical based on the results of the numerical FEM analysis.

During the analysis of the CT results, attention was paid to the zone of the center of the forging (Fig. 10a, b, d). In the part that was formed by the lower die, FEM analysis

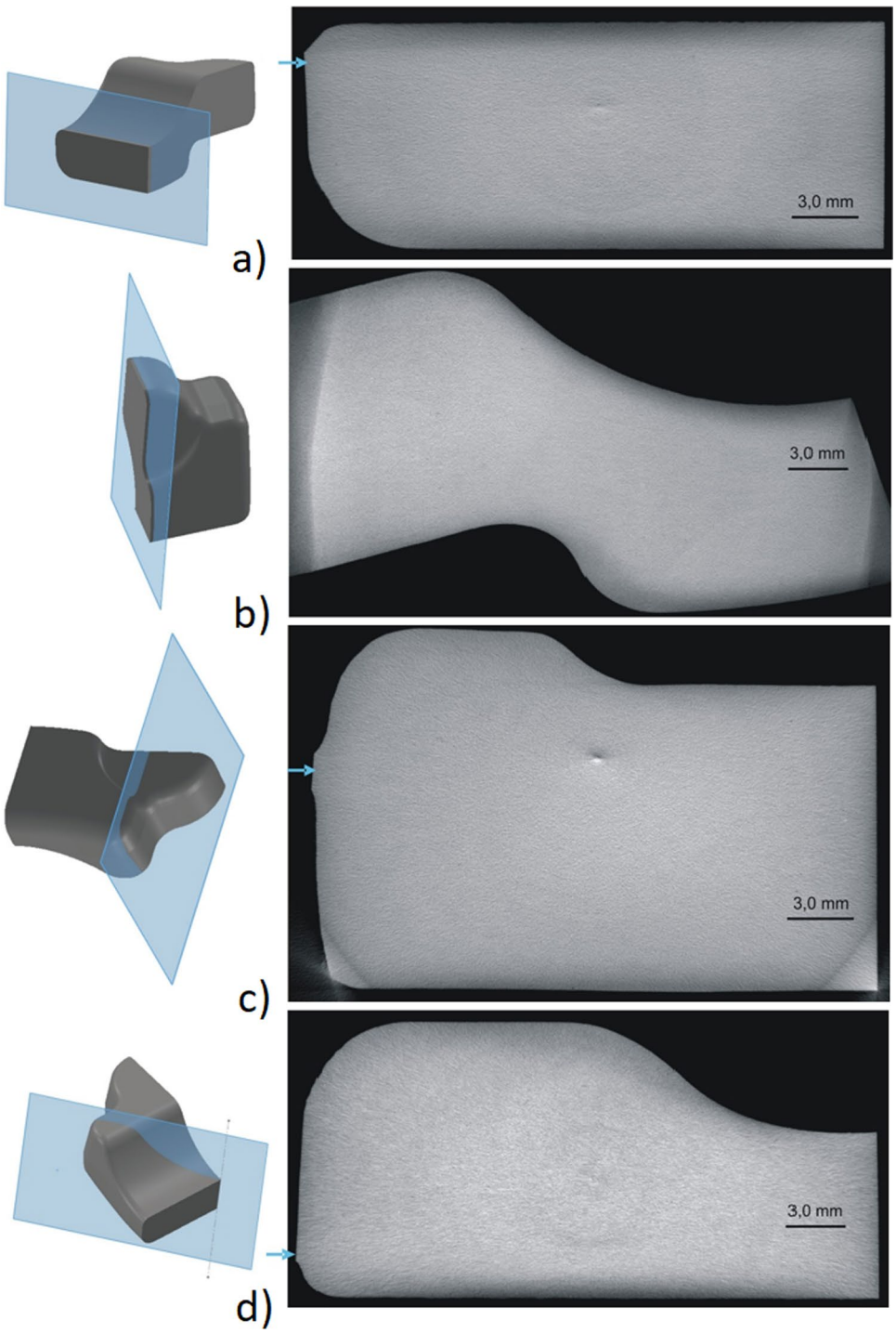

Fig. 10 Diagrams of the location of selected sections of the sintered alloy after forging and the corresponding images of the internal structure of the forging, taken by computed tomography; **a**–**c** linear scanning in directions perpendicular to the planes, **d** rotational scanning with a rotation angle of 0.25°

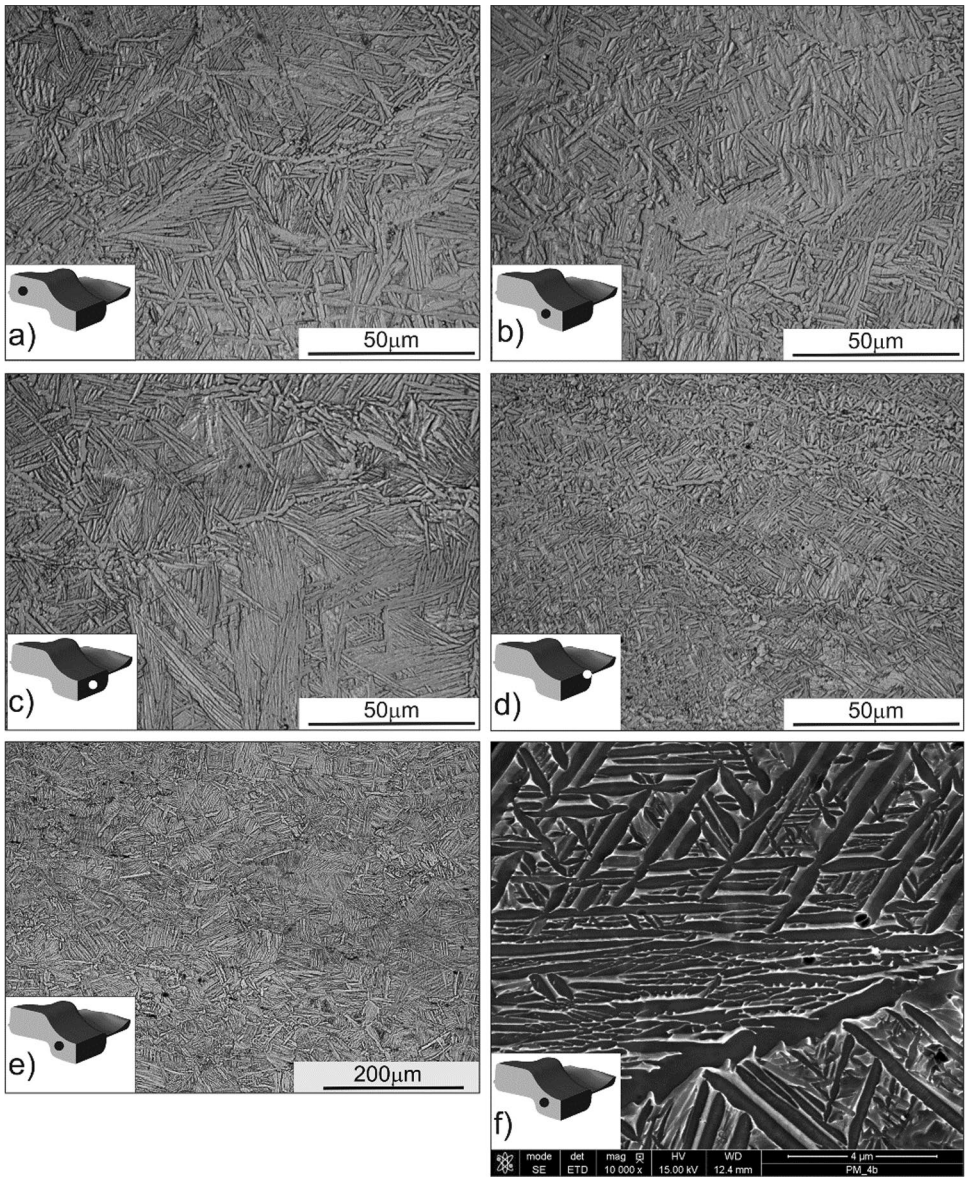

Fig. 11 Microstructure of a Ti–6Al–4V alloy forging, obtained by forging at 1000 °C sintered alloy. Longitudinal sections, etched. Images obtained by: **a–e** light microscopy, **f** scanning electron microscopy

showed the largest temperature drop, and consequently, the maximum value of effective stress. On the other hand, in the part that was formed by the upper die, the FEM analysis showed the presence of maximum values of mean stress. In the aforementioned zones, the strain value was the highest. The FEM modeling showed that the significant deformation, combined with the high tool speed (250 mm s^{-1}), caused a temperature rise in this zone, due to the conversion of the work of plastic deformation into heat. A similar effect was also found in the zones of transition of the forging into the flash (Fig. 10a, c, d). Based on the modeling of the forging process, intermediate areas between zones of varying strain rates were also identified as sensitive (Fig. 10b–d). Also in these zones, CT analysis did not show the presence of laps or microcracks. Nor were pores and discontinuities of a size not smaller than the resolution used found throughout the forging. However, single bright spots were found in some images. They were not visible on adjacent images, indicating that their size did not exceed the scanning resolution of 15 µm. Their presence indicates an increased density of scanned material in these areas.

3.8.2 Microstructure characterization of forgings

Microstructure observations of forgings formed in open dies were carried out using light and scanning microscopy methods. Figure 11 shows images of the microstructure of a sintered alloy forged at 1000 °C, which were taken in selected areas of the forgings and at various magnifications. Figure 12 compares microstructure images of a formed casting under the same conditions. Observations of the microstructure did not reveal the presence of defects in the form

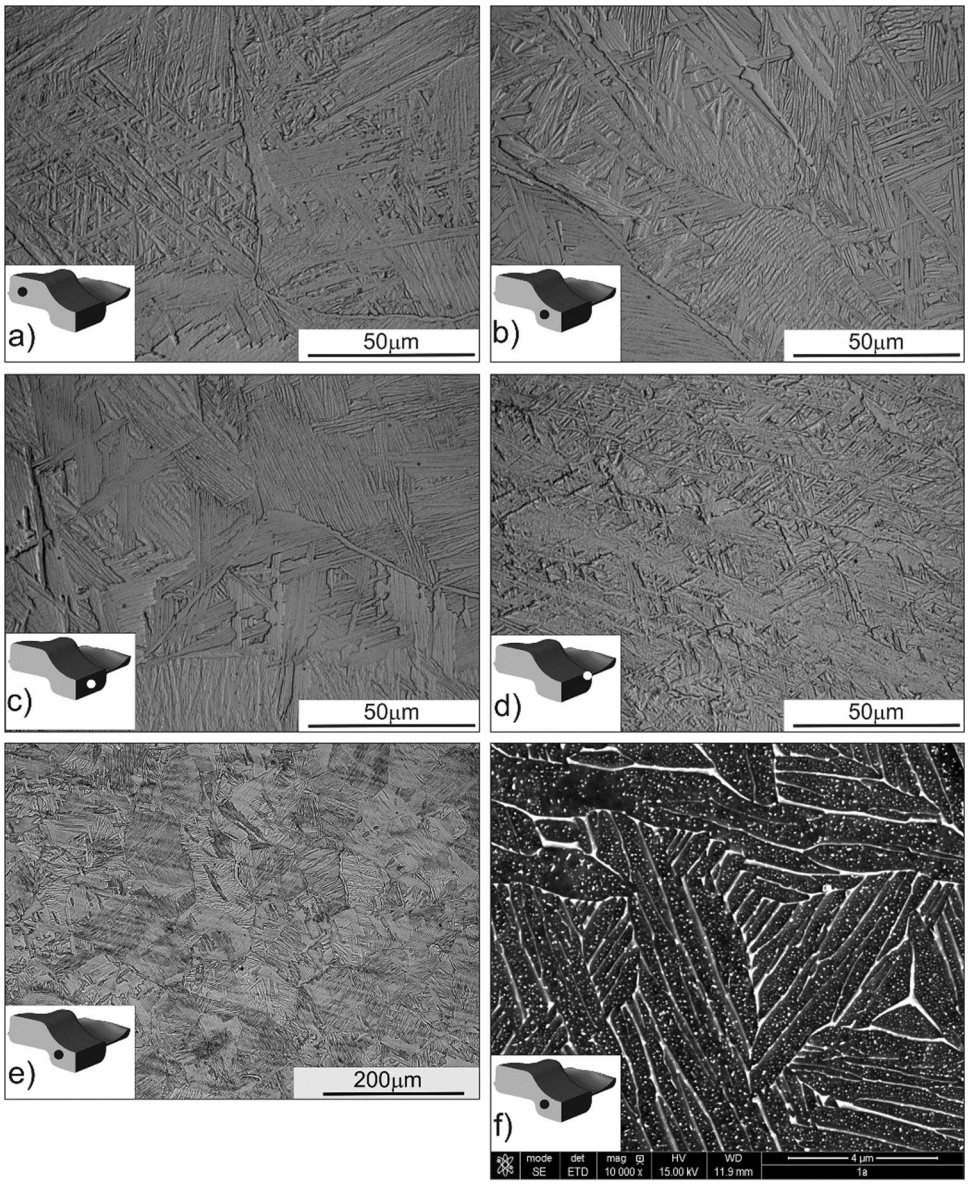

Fig. 12 Microstructure of a Ti–6Al–4V alloy forging obtained by forging at 1000 °C of a cast feedstock. Longitudinal sections, etched. Images obtained by: **a**–**e** light microscopy, **f** scanning electron microscopy

of delaminations or microcracks. It was observed that for both feedstocks manufacturing methods, forging the under the adopted conditions and cooling in air leads to a qualitatively similar microstructure, consisting of α-phase plates in a β-phase matrix and with clearly visible primary grain boundaries of the β-phase. In the case of hot forged sintered alloy, the size of the primary grains is slightly smaller, which is evident when comparing the state of the microstructure in the same areas of the two forgings (Figs. 11 and 12). In the case of these forgings, the plates located at the boundaries of the primary β-phase grains are less massive, and their size is comparable to the α-phase plates found inside these grains. For this reason, the primary grains are less visible than in the case of the forging made from cast feedstock, particularly when observed using lower magnification (Figs. 11e and 12e). The microstructure of the forging obtained from the cast feedstock shows a greater orientation in the zone of transition into the flash (Fig. 12d), which was identified as a sensitive area on the basis of FEM modeling. In the case of the forging obtained by powder metallurgy, a much higher fragmentation of the plates was observed in this zone (Fig. 11d), which is preferred. As a result of the use of feedstock in the form of a sintered alloy, the microstructure observed in different zones of the forging is slightly more homogeneous. However, there was no significant effect of the choice of observation site on the microstructural state of individual forgings (Figs. 11a–c and 12a–c). The exception to this was the flash transition zone of both materials (Figs. 11d, 12d), where the microstructure showed greater fragmentation and orientation than in other areas. A comparison of the microstructure observed at high magnifications using scanning microscopy showed a similar arrangement

of lamellae, with the individual lamellae observed in the sintered alloy after hot forging being slightly more massive, as seen in the comparison in Figs. 11f and 12f.

3.8.3 Hardness of forgings

Hardness measurements were made analogously for forgings produced by both adopted methods, and the resulting hardness distributions were compared. Measurements were made on sections in which the material flow pattern and strain value varied. Diagrams showing the location in the volume of the forging of the areas in which HV_2 measurements were carried out, and the methodology for carrying them out. The obtained hardness distributions are summarized in Fig. 13.

The hardness distributions developed for both forgings show a fairly uniform character (Fig. 13). Slightly elevated HV_2 values were observed in areas near the outer surfaces of the forgings, particularly in the zone adjacent to the surface formed by the upper die. Exceptions to this were the distributions obtained in the case of the forged sintered alloy, in the zones labeled a and c in the diagram (Fig. 13), where local hardness peaks were also found in the middle zone of the forging, with the differences in HV_2 values discussed not being significant. The hardnesses obtained from measurements in three different areas of the forgings had similar values, which were found for both types of tested feedstocks. A comparison of the hardness distributions of the forgings obtained by using different feedstock technologies (Fig. 13a, c, e, and Fig. 13b, d, f) showed that the hardnesses of the forged products from the semi-finished product obtained by powder metallurgy were higher, compared to the HV_2 values obtained in the corresponding areas of the forgings obtained from the cast feedstock. This relationship was observed in all areas of the forgings studied regardless of the location where the measurements were taken. The average difference in hardness ranged from 30 to 45 HV_2 in the studied areas, with local differences in the measurement results at corresponding points having a wider range.

4 Discussion of the results

The starting materials for the sintered alloy were elemental powders of titanium, aluminum, and vanadium, which were dictated by economic considerations. It was assumed that one of the conditions for receiving a high-quality product was to obtain a homogeneous mixture. The powders were mixed in the presence of WC balls (time 120 min, speed 0.9 rpm). Using EDS analysis (Sect. 3.1), the particles of the individual powders were identified, which allowed qualitative evaluation of the uniformity of their distribution and recognition of the effects occurring during mixing. The mixing process in the presence of WC balls resulted in the effect of depositing soft aluminum powder particles on the surfaces of larger and harder titanium and vanadium powder particles. Vanadium was observed in the form of particles and fragments of these particles, crushed, and applied to the surface of titanium particles. The results of the quality assessment of the mixture were satisfactory, as the mentioned effects encourage homogenization of the chemical composition of the alloy during hot pressing.

Semi-finished products from the mixture intended for hot deformation were made by hot pressing (temperature 1200 °C, time 2 h, unit pressure 25 MPa, argon). The microstructure of the resulting sintered alloy had a lamellar structure. It consisted of massive lamellae of α-phase in a matrix of β-phase, as well as α-phase precipitates distributed on the primary grain boundaries of β-phase. The few pores observed were small in size and spherical in shape. The average relative density of the sintered alloy (99.4%) was close to the specific value of the solid material. Therefore, it was assumed that during the planned hot deformation in the following stages (uniaxial compression, forging), the changes in the volume of the sintered alloy caused by compaction would be insignificant. The average value of UTS was 1022 MPa. Since the tensile strength of sinters made of the studied alloy usually does not exceed 950 MPa, therefore, it can be assumed that this value is relatively high. On the other hand, a low average value of elongation of the tested material (5.9%) was found, indicating low ductility. The average hardness of the sintered alloy was 338 HV_2.

Based on the results of the testing of the sintered Ti–6Al–4V alloy (Sect. 3.2), it can be concluded that the method of making them from elemental powders was appropriate. At the stage of designing the production path of the product from elemental powders, it was already assumed that the sintering method of the mixture and its parameters would have a significant impact on the properties of the sintered alloy. Therefore, hot pressing conditions were selected that allowed consolidation of powder particles, homogenization of the chemical composition, and achievement of low porosity. The time required for the effective distribution of alloying elements in titanium depends on the efficiency of diffusion and the phase composition of the alloy, as demonstrated, among others, in the work of Ivasishin et al. [46]. The realization of the process at temperatures in the range of β-phase occurrence promoted homogenization. The self-diffusion of titanium and the diffusivity in titanium of the alloying elements, mainly aluminum, are four orders of magnitude higher in the β phase, compared to the α phase [14, 46, 47]. It was also assumed that too short a time of exposure to temperature could lead to lead to local differences in the amount of individual phases, particularly in the close surroundings of the aluminum and vanadium particles. Therefore, it was necessary to use a long enough time for the interpenetration of the αphase stabilizer into the β

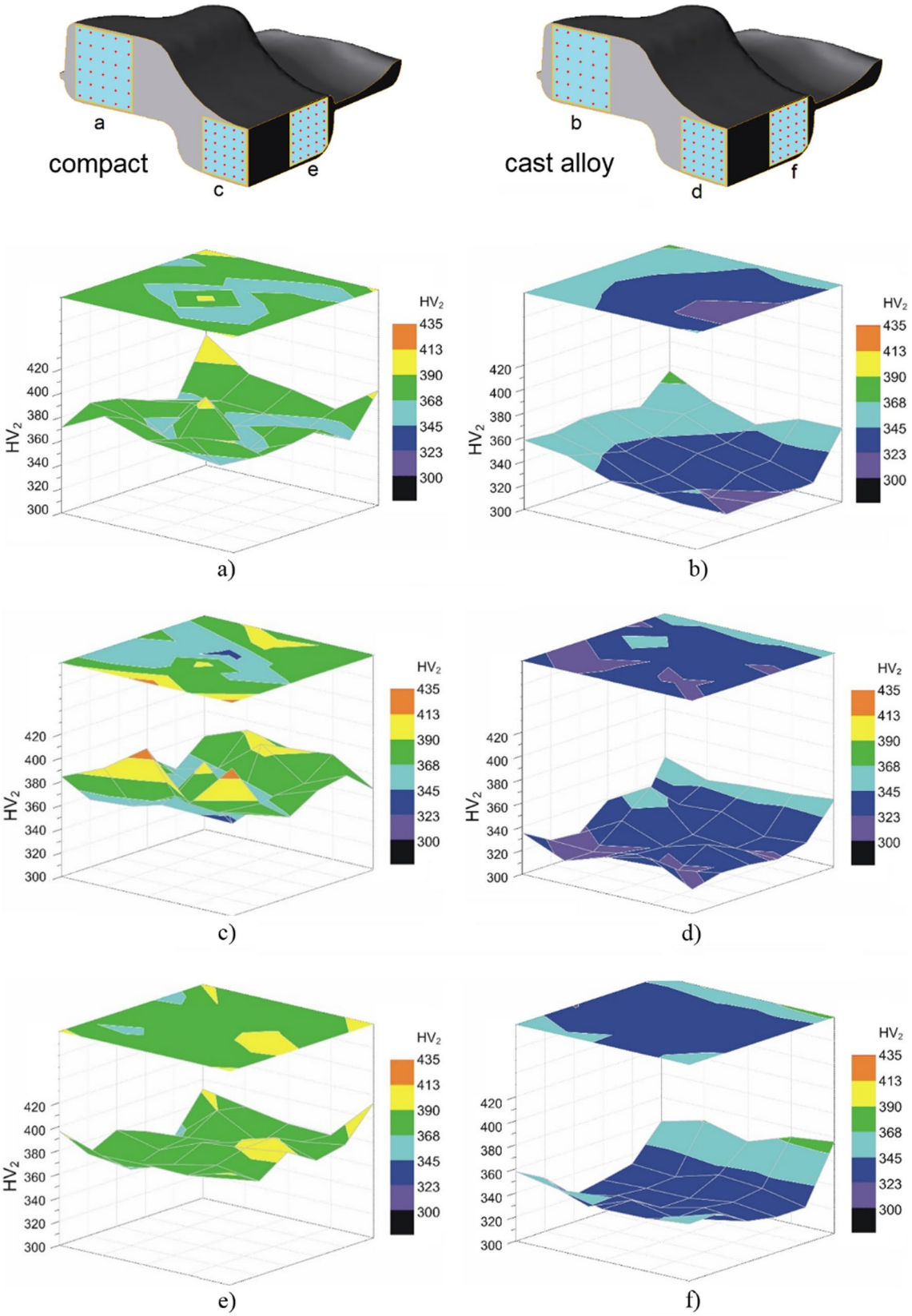

Fig. 13 Diagrams showing the locations of hardness tests on cross-sections of forgings and **a**–**f** HV2 spatial hardness maps

phase and vice versa. Based on the results of microstructure observation and properties evaluation of the sintered alloy, it was confirmed that the hot pressing process carried out under the adopted conditions was adequate to homogenize the chemical composition and eliminate a significant part of the pores. The results obtained indicate that the product produced by the proposed method is suitable as a feedstock for hot plastic processing, including in the die forging process in the β-phase range.

Following the objectives of the work, the results of hot forging in open dies sintered alloy were compared with the results of tests carried out on a reference material, which was a casting and hot-rolled Ti–6Al–4V alloy, in the shape of a bar (Sect. 3.3). The microstructure of this alloy in the as-delivered state is composed of fine equiaxial α-phase grains and β-phase grains lying on the boundaries of α grains. The average values determined in the tensile test were YS = 978 MPa, E = 108 GPa, UTS = 1017 MPa and elongation of 13.5%. The average hardness of the reference material was 317 HV_2. A comparison of the results of the sintered alloy and the reference alloy (Sects. 3.2 and 3.3) showed that the strength properties of both materials determined by tensile tests were similar. The material obtained by powder metallurgy had significantly lower ductility and higher hardness HV_2.

It was assumed that the temperature of the end of the α + β ↔ β phase transformation in titanium alloys is affected not only by their chemical composition but also by the method of their manufacture. Therefore, a study was undertaken leading to the estimation of the end temperature of the phase transformation of the sintered alloy of Ti–6Al–4V alloy. In the first stage, dilatometric tests of heating and cooling were performed. The differential curve developed for heating showed an expansion effect in the temperature range from 300 to 400 °C. It is most likely related to the activation of the diffusion transformation involving the decomposition of the metastable β phase into the α phase. A mild dilatation effect involving inhibition of the expansion rate of the sintered alloy was found above 700 °C. This effect indicates the wide range of occurrence of the α + β ↔ β phase transformation. For this reason, it was not possible to precisely determine the temperature at the end of the phase transformation. To clarify the temperature at the end of the α + β ↔ β transformation, the study was extended to a quantitative analysis of the contribution of α and β phases as a function of temperature. Heating the samples to temperatures in the range of 1000–1010 °C resulted in a small amount of the α phase, around 4%. This result confirms the conclusions made based on the analysis of the dilatometric curves. In the case of samples heated to temperatures in the range of 1020–1030 °C and cooled at a high rate, observations of their microstructure showed only insignificant amounts of the α phase. Based on the results of the study of the phase transformation temperature of the sintered Ti–6Al–4V alloy, it was assumed that the application of a temperature of 1000 °C during forging under dynamic conditions would be sufficient for the almost complete occurrence of the α + β ↔ β transformation, resulting in the lamellar microstructure.

Based on the analysis of the results of hot compression tests on the Gleeble 3800 simulator (Sect. 3.5), the behavior of the Ti–6Al–4V alloy in terms of the occurrence of the β-phase, depending on the strain rate, was determined, and compared. The need to complete information on the behavior of the sintered alloy under high strain rates was considered. The absence in the literature of alloy characteristics under high strain rates, of the order of 100 s^{-1}, was reported by Bruschi et al. [38], and an analysis of more recent literature confirmed that this condition has not changed significantly. The available information mainly concerns alloys obtained from casting process feedstock [38, 48]. This is mainly due to the technical limitations of plastometric test stands. For this reason, in addition to tests in the ranges of low strain rates (0.01–0.1 s^{-1}) and at speeds defined as medium (0.1–10 s^{-1}), tests were also performed at strain rates of 100 s^{-1}. It was assumed that the results obtained will add to the state of knowledge on the behavior of the Ti–6Al–4V alloy during its hot plastic processing. It was also assumed that the results would be useful for designing processes on equipment with dynamic characteristics, such as screw presses or hammers. In the case of the flow curve obtained by hot compression at a strain rate of 100 s^{-1}, the oscillatory character of its course over the full range of deformations was found. This effect for titanium alloys has already been demonstrated in several other works, both when studying materials produced by casting processes [38, 48] and those obtained by powder metallurgy methods [36, 49, 50]. In the case of the studied material, a possible reason for the imbalance between the strengthening effect and the compensating softening of the material under these conditions is the conversion of the work of plastic deformation into heat. Flow curves developed from compression tests at strain rates in the range of average strain rates from 1 to 100 s^{-1}, showed a decrease in the value of real stress over the full strain range. In the case of low strain rates, in the range of 0.01–0.1 s^{-1}, strain growth occurred with a slightly decreasing value of true stress. The curves obtained under these test conditions did not show a strengthening effect, and their course was similar, differing only in the values of true strain.

Analysis of the results of FEM modeling of the die forging process of a product with the adopted shape and with the conditions selected as favorable (Sect. 3.6) indicated the possibility of correct filling of the die and, as a result, obtaining a product free of forging defects such as laps. Analysis of the temperature distribution in the final forging stage showed that significant temperature increases, due to the conversion

of plastic deformation work into heat, are to be expected only in the area immediately adjacent to the flash and in the flash zone. This is due to the intense flow of material in the mentioned areas. In the rest of the forging volume, the FEM analysis did not show temperature rises above 1080 °C. A temperature drop slightly below 1000 °C occurred only in the zone near the contact surface of the feedstock with the lower die, which was due to the significant difference in the temperatures of the feedstock and the tool. The consequences of this are the relatively high values of effective stress found in this area, which is necessary to force the material to flow at a lower temperature and, therefore, under conditions of reduced plasticity. The highest values of effective stress were observed in the zone in the area adjacent to the flash and in part of the flash itself. In this area, the flow of material outside the die to flash requires overcoming the frictional force at the contact surface between the shaped alloy and the tool and is significantly hindered. In contrast, outside these areas in the forging volume, the value of effective stress was relatively low. Positive values of mean stress were observed only in the flash zone, while compressive stresses were present in the rest of the forging. The highest values of these stresses were found in the central part of the forging, especially in the part shaped by the upper die and at the rounding of the die. This may indicate that friction at the contact surface between the material and tools in these zones will impede plastic flow. The result could be accelerated tool wear in these areas and even a failure of the forged material. FEM modeling results also indicate that another potentially sensitive area in the forging volume is the flash contact zone. The reasons for this are differences in the value of mean stress and very large variations in the value of strain. In the rest of the forging volume, the distribution of strain values was fairly uniform, which is favorable. The results of FEM modeling showed that the realization of the forging process of the selected shape and under the conditions adopted during the simulation leads to the correct filling of the die. However, the analysis of the obtained results also made it possible to select those areas in the volume of the forging that, during the realization of the modeled process under industrial conditions, are particularly vulnerable to the occurrence of possible defects, including laps or cohesion violations. Therefore, after the technological tests of forging, the quality of the forging in these areas should be subjected to strict control.

The correctness of the tests obtained at this stage was verified by performing forging tests on an industrial line (Sect. 3.7) and then evaluating the microstructural state and selected properties of the forgings (Sect. 3.8). The tests were conducted under conditions determined to be favorable based on dilatometric studies, calculations of the proportion of alpha and β phases as a function of temperature, and FEM modeling results. A feedstock in the form of sintered alloy was used, as well as a reference material, which was a commercially used casting and hot-rolled Ti–6Al–4V alloy.

The initial visual evaluation of the forgings showed no noticeable defects on their external surfaces. It was found that as a result of the implementation of hot forging tests in the range of β-phase occurrence and with high speed of tool movement, the proper filling of the die occurred. Regardless of the method of making the feedstock, products with the correct shape were obtained. Cracks were observed only in the flash zone of forgings made from both types of feedstock. This is consistent with the results of the FEM modeling, during which this zone was indicated as particularly prone to the occurrence of defects. However, this fact does not affect the quality of the products, since the flash represents waste and is removed.

During CT testing of the forging made of powders (Sect. 3.8.1), special attention was paid to the state of the internal structure of those areas that were selected as sensitive based on the results of numerical FEM analysis. It was assumed that in the case of the occurrence in the forging of defects with an equiaxial shape and with dimensions smaller than the applied resolution of 15 µm, such as pores, they may not have been registered. However, such a danger does not apply to defects in the form of delaminations or cracks, which pass through many sections and are, therefore, easy to identify with the CT method. Testing along two mutually perpendicular axes and the use of additional rotational scanning excluded the possibility of hiding such defects due to their orientation according to the scanning axis. The CT results of the forging confirmed the result of the initial assessment of its quality made immediately after forging, which testified to its correct execution. The CT analysis showed no laps or microcracks. There were also no pores or discontinuities with a size not smaller than the resolution used. Analysis of the CT results of the forging showed the presence of single bright spots on some images. They were usually visible on single images and were not observed on adjacent images. This indicates that their size did not exceed the scanning resolution. Their presence may be due to the increased density of the scanned material in these areas, indicating an increased concentration of an element with a density higher than that inherent in the Ti–6Al–4V alloy, in this case, vanadium. A possible reason for this is the incomplete diffusion of vanadium in these areas from the primary powder particles of this element into the alloy during hot pressing and forging. However, the tomograms showed no darker zones, indicating a local concentration of a lower density element, which is aluminum. This demonstrates the uniform diffusion of this element into the alloy matrix during the hot pressing process.

Microstructural studies of the forgings (Sect. 3.8.2) showed that for both methods of manufacturing the feedstock, its forging under the adopted conditions and cooling

of the forgings in the air led to a microstructure, consisting of α-phase plates in a β-matrix and with clearly visible primary β grain boundaries. This is the microstructure, the obtaining of which was one of the main objectives of the research undertaken. The observed microstructure was similar for both types of feedstock. The only significant difference was the slightly smaller size of the primary β grains found for the sintered alloy after hot forging. Also, a comparison of the microstructure state carried out at high magnification by scanning microscopy showed a similar shape of the plates and a similar arrangement concerning each other. Differences were observed only in the size of the plates, which were thicker in the case of the powder product. According to the assumptions made in the study, no heat-treatment leading to homogenization of the microstructure of the feedstock was performed, so the microstructure of the forging feedstocks of the two compared materials depended on the method of their manufacture and differed significantly. Nevertheless, as a result of heating the materials to the assumed temperature, forging them under the assumed conditions (β-phase range and high strain rate), and then cooling the forgings in air, products with similar microstructure were obtained. This observation leads to the conclusion that, within the range of the studied parameters, the conditions of the successive operations, i.e., the heating of the feedstock, forging process, and the cooling of the product after forging, have a decisive influence on the microstructural state of the forgings. Another important observation comes from comparing the microstructure at different locations in the forging volume. As a result of this comparison, there was no significant effect of the choice of observation location on its condition. This is consistent with the forgings made by both proposed methods. The shape of the die adopted for testing caused the deformation to vary in volume and forced the material to flow unevenly. However, the effects of such differentiation, except the flash zone, were not observed. This leads to the conclusion that during cooling in air, full recrystallization occurs, removing the effect of microstructure orientation caused by plastic flow and its homogenization in the volume of the forging. A similar effect was observed during studies on cast alloy by Astarita et al. [39]. The exception to this was, for both materials, the flash transition zone, where the microstructure showed greater fragmentation and orientation than in other areas. However, in this area, the mean stress values are positive, and there are high values of strain. It should also be noted that the flash represents technological waste, which is removed immediately after forging. Taking into account the results of microstructural observations, it can be concluded that during forging under dynamic conditions, a temperature of 1000 °C, which is only slightly higher than the phase transformation temperature, is appropriate. Its application during forging at a high strain rate of Ti–6Al–4V alloy feedstock produced by both methods leads to the assumed microstructure with lamellar structure.

The hardness distributions developed for forgings formed on a screw press (Sect. 3.8.3) showed a fairly uniform character. Slightly elevated HV_2 values were observed in areas lying near the outer surfaces of the forgings, mainly in the zone adjacent to the surface shaped by the upper die. In the case of the forged sintered alloy, local hardness peaks were also found in the center zone of the forging. However, the aforementioned differences were insignificant, and therefore, it should be assumed that the hardnesses of the two tested forgings measured in their different areas had quite similar values. These results are consistent with metallographic observations of the forgings, which showed a lack of microstructural variation in these areas. A comparison of the HV_2 distributions of forgings obtained by using different feedstock manufacturing technologies showed that the hardnesses of forged products using an intermediate product obtained by powder metallurgy were higher, compared to the HV_2 values obtained for the cast feedstock. This relationship was observed in all areas of the forgings studied and regardless of where the measurement was performed. The average difference in hardness seen in the comparison ranged from 30 to 45 HV_2, and local differences in the measurement results at the corresponding points had a wider range. The likely reason for the higher hardness of the product obtained by powder metallurgy was the presence in its microstructure of fragmented oxides from the surface of the original powder particles. Higher HV_2 values of the forging received in this way may also be influenced by the slightly higher size of the α-phase plates. Such a tendency may also be favored by the greater fragmentation during the forging process of the primary grains of the β-phase, on the boundaries of which the α-phase was precipitated.

The absence of significant differences in microstructural state and hardness values on cross-sections of forgings with varying degrees of deformation relative to each other indicates that the forging conditions, developed based on FEM modeling results, were correct. Proper process design also confirms the absence of surface or internal defects in the microstructure of the forgings, such as cracks, which is also consistent with the results of CT testing of the sintered alloy.

The summary of the research conducted in general allows to conclude that the significant effect was the comprehensive development of guidelines for the implementation of the forging process in the β-phase range and at a high strain rate of the Ti–6Al–4V alloy obtained from elemental powders, the use of which under industrial conditions led to the production of defects-free forgings with a controlled, favorable microstructure. To achieve this goal, numerical modeling using the finite element method was used, an approach rarely

used in the design of forging technologies for semi-finished products obtained by powder metallurgy. The use of FEM modeling allowed for the correct design of the forging process of the studied alloy, considering the conditions and limitations present in the industrial line. The economic aspect is also an important factor. At present, expensive alloy powders or mixtures of titanium powder and Al-V alloy powder are mostly used to manufacture Ti–6Al–4V alloy products by powder metallurgy. A consequence of the choice of less expensive elemental powders was to ensure homogenization of the chemical composition of the sintered alloy. This was achieved by following a proper mixing procedure and a correct method of consolidating the mixture. It was shown that hot forging of sintered alloy leads to products with microstructure and properties comparable to those obtained for cast feedstock, which was confirmed in tests on an industrial line and comparative studies of forgings. According to the authors, these results are crucial since the requirement for the implementation of alternative technology is not only the economic aspect but also the quality of the product, which must not significantly differ from the quality of products obtained using commercial processes.

5 Conclusions

The results of the study of the forging process in open dies of Ti–6Al–4V alloy obtained from elemental powders, which was carried out in the β-phase range and at a high strain rate, led to the following conclusions:

1. Based on the results of dilatometric tests supported by quantitative analysis of the volume fraction of α and β phases as a function of temperature, it is shown that forging of sintered alloy at 1000 °C will be sufficient for the almost complete occurrence of $\alpha+\beta \leftrightarrow \beta$ transformation, and as a result to obtain the assumed lamellar microstructure.
2. The FEM analysis of the die forging process of as-sintered Ti–6Al–4V alloy in the β-phase range and at a high strain rate enabled the determination of conditions leading to the correct filling of die and allowed the selection of those areas in the volume of the forging that are particularly prone to the occurrence of defects during the implementation of the process under industrial conditions.
3. Forging tests in open dies at 1000 °C and on a screw press operating at a maximum speed of 250 mm s^{-1}, which were carried out for sintered alloy and commercially used feedstock in the form of rolled casting, led to products free of defects. It was confirmed that the sintered alloy made by the proposed method is suitable as a feedstock for hot-forming processes in the β-phase range. It was also shown that the forgings obtained from it do not differ in quality from that made from the reference material.
4. Forging under the proposed conditions of semi-finished products with significantly different microstructures led to the production of forgings with uniform and similar lamellar microstructures. Thus, it was shown that the conditions for heating the feedstock, the parameters of its forging process, and the method of cooling the product after forging have a decisive effect on the microstructure state of forgings shaped in the β-phase range.
5. The conducted dilatometric tests, plastometric tests and the results of numerical FEM modeling conducted provided guidelines that, at the stage of designing the forging process under the adopted conditions, allowed a controlled, favorable microstructure of the Ti–6Al–4V alloy product obtained from elemental powders.

Funding This research received no external funding.

Data Availability The data that support the findings of this study are available from the corresponding author upon reasonable request.

Declarations

Conflict of interest The authors have no conflicts of interest to declare that are relevant to the content of this article.

Ethical approval This article does not contain any studies with human participants or animals performed by any of the authors.

References

1. Motyka M. Titanium alloys and titanium-based matrix composites. Metals. 2021;11(9):1463.
2. Majorell A, Srivatsa S, Picu RC. Mechanical behavior of Ti6Al4V at high and moderate temperatures—part I: experimental results. Mater Sci Eng A. 2002;326(2):297–305.
3. Cui C, Hu BM, Zhao L, Liu S. Titanium alloy production technology, market prospects and industry development. Mater Des. 2011;32(3):1684–91.

4. Ziaja W, Motyka M, Kubiak K, Sieniawski J. Primary creep behaviour of two-phase titanium alloy with various microstructure. Arch Metall Mater. 2016;61(2):683–8. https://doi.org/10.1515/amm-2016-0116.
5. Jiang YQ, Lin YC, Wang GQ, Pang GD, Chen MS, Huang ZC. Microstructure evolution and a unified constitutive model for a Ti-55511 alloy deformed in β region. J Alloys Compd. 2021;870:159534.
6. Liu YX, Chen W, Li ZQ, Tang B, Han XQ, Yao G. The HCF behavior and life variability of a Ti–6Al–4V alloy with transverse texture. Int J Fatigue. 2017;97:79–87.
7. Li G, Sun C. High-temperature failure mechanism and defect sensitivity of TC17 titanium alloy in high cycle fatigue. J Mater Sci Technol (Shenyang, China). 2022;122:128–40.
8. Khan MA, Williams RL, Williams DF. In-vitro corrosion and wear of titanium alloys in the biological environment. Biomaterials. 1996;17:2117–26.
9. Zhou X, Xu D, Geng S, Fan Y, Yang C, Wang Q, Wang F. Microstructural evolution and corrosion behavior of Ti–6Al–4V alloy fabricated by laser metal deposition for dental applications. J Mater Res Technol. 2021;14:1459–72.
10. Kaur M, Singh K. Review on titanium and titanium based alloys as biomaterials for orthopedic applications. Mater Sci Eng C. 2019;102:844–62.
11. Szkliniarz W, Chrapoński J, Kościelna A, Serek B. Substructure of titanium alloys after cyclic heat treatment. Mater Chem Phys. 2003;81:538–41.
12. Yan-Wei S, Zhi-Meng G, Jun-Jie H, Dong-Hua Y. Effect of spheroidization of Ti–6Al–4V powder on characteristics and rheological behaviors of gelcasting slurry. Procedia Eng. 2012;36:299–306.
13. Heinl P, Müller L, Körner C, Singer RF, Müller FA. Cellular Ti–6Al–4V structures with interconnected macro porosity for bone implants fabricated by selective electron beam melting. Acta Biomater. 2008;4:1536–44.
14. Bolzoni L, Ruiz-Navas EM, Gordo E. Flexural properties, thermal conductivity and electrical resistivity of prealloyed and master alloy addition powder metallurgy Ti–6Al–4V. Mater Des. 2013;52:888–95.
15. Haase C, Lapovok R, Ng HP, Estrin Y. Production of Ti–6Al–4V billet through compaction of blended elemental powders by equal-channel angular pressing. Mater Sci Eng A. 2012;550:263–72.
16. Boyer R, Welsch G, Collings EW. Materials properties handbook: titanium alloys. Materials Park: ASM International; 1994.
17. Szkliniarz A, Szkliniarz W. Effect of carbon content on the microstructure and properties of Ti–6Al–4V alloy. Arch Metall Mater. 2020;65(3):1197–204.
18. Weston NS, Jackson M. FAST-forge—a new cost-effective hybrid processing route for consolidating titanium powder into near net shape forged components. J Mater Process Technol. 2017;243:335–46.
19. Motyka M. Martensite formation and decomposition during traditional and AM processing of two-phase titanium alloys—an overview. Metals. 2021;11:481. https://doi.org/10.3390/met11030481.
20. Verleysen P, Peirs J. Quasi-static and high strain rate fracture behaviour of Ti6Al4V. Int J Impact Eng. 2017;108:370–88.
21. Lei L, Zhao Y, Zhao Q, Wu C, Huang S, Jia W, Zeng W. Impact toughness and deformation modes of Ti–6Al–4V alloy with different microstructures. Mater Sci Eng A. 2021;801:140411.
22. Wojtaszek M, Śleboda T, Czulak A, Weber G, Hufenbach WA. Quasi-static and dynamic tensile properties of Ti–6Al–4V alloy. Arch Metall Mater. 2013;58(4):1261–5.
23. Semiatin SL, Goetz RL, Seetharaman V, Shell EB, Ghosh AK. Cavitation and failure during hot forging of Ti–6Al–4V. Metall Mater Trans A. 1999;30(5):1411–24.
24. Warwick JLW, Jones NG, Bantounas I, Preuss M, Dye D. In situ observation of texture and microstructure evolution during rolling and globularization of Ti–6Al–4V. Acta Mater. 2013;61(5):1603–15.
25. Seshacharyulu T, Medeiros SC, Frazier WG, Prasad YVRK. Microstructural mechanisms during hot working of commercial grade Ti–6Al–4V with lamellar starting structure. Mater Sci Eng A. 2002;325(1–2):112–25.
26. Careau SG, Tougas B, Ulate-Kolitsky E. Effect of direct powder forging process on the mechanical properties and microstructural of Ti–6Al–4V ELI. Materials. 2021;14:4499.
27. Wojtaszek M, Korpała G, Śleboda T, Zyguła K, Prahl U. Hot processing of powder metallurgy and wrought Ti−6Al−4V alloy with large total deformation: physical modeling and verification by rolling. Metall Mater Trans A. 2020;51(11):5790–805.
28. Wojtaszek M, Śleboda T. Thermomechanical processing of P/M Ti–6Al–4V alloy. In: METAL 2013, 22nd international conference on metallurgy and materials. Ostrava: TANGER; 2013. p. 364–69.
29. Qiu JW, Liu Y, Liu B, Liu YB, Wang B, Ryba E, Tang HP. Optimizing the hot-forging process parameters for connecting rods made of PM titanium alloy. J Mater Sci. 2012;47:3837–48.
30. Kanou O, Fukada N, Hayakawa M. The effect of Fe addition on the mechanical properties of Ti–6Al–4V alloys produced by the prealloyed powder method. Mater Trans. 2016;57(5):681–5.
31. Liang C, Ma MX, Jia MT, Raynov S, Yan JQ, Zhang DL. Microstructures and tensile mechanical properties of Ti–6Al–4V bar/disk fabricated by powder compact extrusion/forging. Mater Sci Eng A. 2014;619:290–9.
32. Jia M, Zhang D, Liang J, Gabbitas B. Porosity, microstructure, and mechanical properties of Ti–6Al–4V alloy parts fabricated by powder compact forging. Metall Mater Trans A. 2017;48:2015–29.
33. El-Soudani SM, Yu K, Crist EM, Sun F, Campbel MB, Esposito TS, Phillips JJ, Moxon V, Duz VA. Optimization of blended-elemental powder-based titanium alloy extrusions for aerospace applications. Metall Mater Trans A. 2013;44:890–910.
34. Froes FH. Powder metallurgy of titanium alloys, vol. 1. Amsterdam: Elsevier; 2013. p. 202–40.
35. Hu H, Xu Z, Dou W, Huang F. Effects of strain rate and stress state on mechanical properties of Ti–6Al–4V alloy. Int J Impact Eng. 2020;145: 103689.
36. Wang G, Xu L, Wang Y, Zheng Z, Cui Y, Yang R. Processing maps for hot working behavior of PM alloy. J Mater Sci Technol (Shenyang, China). 2011;27:893–8.
37. Fang XR, Wu J, Ou X, Yang FQ. Microstructural characterization and mechanical properties of Ti–6Al–4V alloy subjected to dynamic plastic deformation achieved by multipass hammer forging with different forging temperatures. Adv Mater Sci Eng. 2019;2019:1–12.
38. Bruschi S, Poggio S, Quadrini F, Tata ME. Workability of Ti–6Al–4V alloy at high temperatures and strain rates. Mater Lett. 2004;58(27–28):3622–9.
39. Astarita A, Ducato A, Fratini L, Paradiso V, Scherillo F, Squillace A, Testani C, Velotti C. Beta forging of Ti–6Al–4V: microstructure evolution and mechanical properties. Key Eng Mater. 2013;554–557:359–71.
40. Lee DG, Lee S, Lee CS, Hur S. Effects of microstructural factors on quasi-static and dynamic deformation behaviors of Ti–6Al–4V alloys with Widmanstätten structures. Metall Mater Trans A. 2003;34(11):2541–8.
41. Pang GD, Lin YC, Jiang YQ, Zhang XY, Liu XG, Xiao YW, Zhou KC. Precipitation behaviors and orientation evolution

mechanisms of α phases inTi-55511 titanium alloy during heat treatment and subsequent hot deformation. Mater Charact. 2020;167: 110471.
42. Roy S, Suwas S. The influence of temperature and strain rate on the deformation response and microstructural evolution during hot compression of a titanium alloy Ti–6Al–4V–0.1B. J Alloys Compd. 2013;548(4):110–25.
43. Abbasi SM, Momeni A. Effect of hot working and post-deformation heat treatment on microstructure and tensile properties of Ti–6Al–4V alloy. Trans Nonferrous Met Soc China. 2011;21(8):1728–34.
44. Rao KP, Prasad YVRK. Advanced techniques to evaluate hot workability of materials. In: Comprehensive materials processing, vol. 3. Oxford: Elsevier Ltd; 2014. p. 397–426.
45. Guo RP, Xu L, Zong BY, Yang R. Preparation and ring rolling processing of large size Ti–6Al–4V powder compact. Mater Des. 2016;99:341–8.
46. Ivasishin OM, Eylon D, Bondarchuk VI, Savvakin DG. Diffusion during powder metallurgy synthesis of titanium alloys. Book series. Defect Diffus Forum. 2008;277:177–85.
47. Cantin G, Stone N, Alexander D, Gibson M, Ritchie D, Wilson R, Yousuff M, Rajakumar R, Rogers KJ. Production of Ti–6Al–4V strip by direct rolling of blended elemental powder. Mater Sci Forum. 2010;654–656:807–10.
48. Łukaszek-Sołek A, Krawczyk J. Processing maps of the Ti–6Al–4V alloy in a forging process design. Key Eng Mater. 2015;641:190–5.
49. Ning Z, Fu MW, Hou H, Yao Y, Guo H. Hot deformation behavior of Ti–5.0Al–2.40Sn–2.02Zr–3.86Mo–3.91Cr alloy with an initial lamellar microstructure in the α + β phase field. Mater Sci Eng A. 2011;528:1812–8.
50. Ning YQ, Xie BC, Liang HQ, Li H, Yang XM, Guo HZ. Dynamic softening behavior of TC18 titanium alloy during hot deformation. Mater Des. 2015;71:68–77.